

The maximum radiated energy and final spin of high speed collision of two black holes

James Healy, Alessandro Ciarfella, and Carlos O. Lousto

*Center for Computational Relativity and Gravitation,
School of Mathematical Sciences, Rochester Institute of Technology,
85 Lomb Memorial Drive, Rochester, New York 14623, USA*

(Dated: April 29, 2025)

We performed a series of 769 full numerical simulations of high energy collision of black holes to search for the maximum gravitational energy emitted E_{rad} , during their merger. We consider equal mass binaries with spins pointing along their orbital angular momentum \vec{L} and perform a search over impact parameters b and initial linear momenta $p/m = \gamma v$ to find the maximum E_{rad} for a given spin \vec{S} . The total radiated energy proves to have a weak dependence on the intrinsic spin s of the holes, for the sequence $s = +0.8, 0.0, -0.8$ studied here. We thus estimate the maximum $E_{rad}^{max}/M_{ADM} \approx 32\% \pm 2\%$ for these direct merger encounters. We also explore the radiated angular momentum and the maximum spin of the merger remnant (within these configurations), finding $\alpha_f^{max} = 0.987$. We then use the zero frequency limit expansion to analytically model the radiated energy in the small impact parameter and large initial linear momentum regime.

PACS numbers: 04.25.dg, 04.25.Nx, 04.30.Db, 04.70.Bw

I. INTRODUCTION

The extreme scenario of high energy collision of black holes has been the subject of detailed studies in the realm of high-energy colliders to help discover the fundamental laws of nature [1, 2], with applications to the gauge/gravity duality and holography [3], as well as tests of the radiation bounds theorems and cosmic censorship conjecture in General Relativity [4–6], and with regards to primordial black hole collisions in the early universe [7–9].

The high energy scenario was studied with full numerical techniques in [10] to compute the maximum energy radiated by equal mass, nonspinning black holes in an ultrarelativistic headon collision. This study was then followed up [11] by the claim that the spin effects did not matter for these collisions. In [12] we revisited the headon scenario using our new initial data [13] with low spurious initial radiation content for more accurate estimates of the maximum energy radiated, placing it at about 13%. Non headon high energy collisions have been studied in [14] and then with notable analytic detail in [15]. Some of the early reviews on the subject are [1, 2] and a more up-to-date one in [16–18]. Also, interestingly, the scattering of two nonspinning black holes may lead to their spinup during their short term interactions [19].

In a previous work [20] we explored the maximum recoil velocity of such high energy black hole encounters by performing a search in the 4-dimensional parameter space of impact parameters b , linear momentum (per horizon mass) γv , and spins magnitude and orientations in the orbital plane, finding the maximum recoil velocity of the final merged black hole to be about 10% the speed of light.

Here we come back to this high energy collision scenario and target our studies to the search for the maximum achievable radiated gravitational energy from these

grazing, high energy collisions and merger of binary black holes, where now the spin orientation of the holes play a different (as we will see, less relevant) role than in the computation of the recoil. We will perform supercomputer simulations by directly solving fully numerically the General Relativity field equations and supplement their results with analytic computations in the zero frequency limit (ZFL) [15, 21] to fit those results.

II. TECHNIQUES

In order to perform the full numerical simulations we have used the LazEv code[22] with 8th order spatial finite differences [23], 4th order Runge-Kutta time integration with a Courant factor ($\Delta t/\Delta x = 1/4$) implementation of the moving puncture approach [24]. To compute the numerical (Bowen-York) initial data, we use the TWOPUNCTURES [25] code. We use the AHFINDERDIRECT code [26] to locate apparent horizons and measure individual masses m_H and the magnitude of the horizon spin S_H , using the *isolated horizon* algorithm as implemented in Ref. [27].

The CARPET mesh refinement driver provides a “moving boxes” style of mesh refinement. The grid structure of our mesh refinements have a size of the largest box for all simulations of $\pm 400M$. The number of points between 0 and 400 on the coarsest grid is 100 for a resolution of n100. So, the grid spacing on the coarsest is $4M$. The resolution in the wavezone (two refinement levels below the coarsest) is $1M$ (i.e. n100 has $M/1.00$). The grid around the (equal mass) black holes is fixed at $\pm 0.3M$ in size and is the 9th refinement level. Therefore the grid spacing at the finest resolution is $M/256$.

The extraction of gravitational radiation from the numerical relativity simulations is performed using the formulas (22),(23),(24) from [28] for the energy and linear

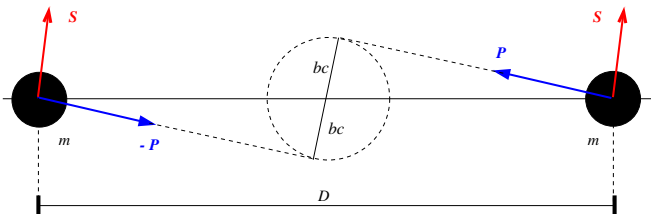


FIG. 1. Initial configurations of the high energy collisions of black holes. With $s = s^z = 0.0, \pm 0.8$ and $D = 50M$.

and angular momentum radiated, respectively, in terms of the extracted Weyl scalar Ψ_4 at the observer location sphere $R_{obs} = 113M$. We then analytically [29] extrapolate expressions for $r\psi_4$ from this finite observer location R_{obs} to \mathcal{I}^+ . To compute Energy, angular and linear momenta radiated from the waveforms we will subtract, in the time domain, at a post-processing stage, the initial burst of spurious Bowen-York data radiation content reaching the observer, to thus obtain more physical values.

III. NUMERICAL RESULTS

In [20] we have explored the maximum the recoil from equal mass binary black holes with opposite spins on the orbital plane. We have designed simulations to explicitly model the problem in terms of the Bowen-York initial linear momentum per horizon mass of the holes, $\gamma v = p/m_H$, (with $\gamma = (1 - v^2)^{-1/2}$, the Lorentz factor, and the horizon area $A_H = 16\pi m_{irr}^2$ providing $m_H^2 = m_{irr}^2 + S_H/4m_{irr}^2$), dimensionless (per unit mass M) impact parameter, b , and spin, $\vec{s} = \vec{S}_H/m_H^2$ (where $m_H = m_{1,2}$ is the horizon mass of each hole) magnitude and orientation, i.e. a four dimensional parameter search.

Here we will supplement that study of black holes high energy collisions by a search of the maximum radiated energy (and final black hole spin). Our simulations families consist of equal mass black holes with spins aligned (or counter-aligned) with the orbital angular momentum \vec{L} , and of an initial spin magnitude, $s = 0.0, \pm 0.8$, for each of the holes as displayed in Fig. 1. We will then explore different initial relativistic velocities (or momentum per mass), γv , and (normalized by M) impact parameters, b , as measured from the initial separation of the holes, $D = 50M$ (with $M = M_{ADM}$, the total Arnowitt-Deser-Misner (ADM) mass of the system [30]). Note that here $m_1 + m_2 = M_{ADM} - E_b$, the addition of the horizon masses of the system, does not add up to 1 (as was normalized in [20]), but here differs from the normalized $M_{ADM} = 1$ by the (negative) initial binding energy, E_b .

The value for the impact parameter b_{max} that leads to the maximum energy radiated (or maximum spin of the merged black hole) corresponds closely to the critical value of the impact parameter b_c separating the direct merger from the scattering of the holes. Those two fam-

TABLE I. Corrections to the maximum E_{rad} due to the initial spurious burst of radiation

spin	b	E_{rad}	E_{rad} -spurious	difference
-0.8	1.40	0.273819	0.246259	-0.027560
-0.8	1.50	0.269910	0.246511	-0.023399
-0.8	1.60	0.269365	0.250295	-0.019070
-0.8	1.75	0.230099	0.216861	-0.013238
0.0	1.30	0.268583	0.234700	-0.033883
0.0	1.35	0.272209	0.244980	-0.027229
0.0	1.40	0.274504	0.249464	-0.025040
0.0	1.50	0.266362	0.249038	-0.017324
0.0	1.65	0.249796	0.239010	-0.010786
+0.8	1.25	0.217894	0.187761	-0.030133
+0.8	1.30	0.261063	0.235021	-0.026042
+0.8	1.40	0.220289	0.211261	-0.009028

ilies being separated by a set of elliptic orbits. A similar analysis can be done to complete this two parameters search by varying the initial velocity (or linear momentum per horizon mass) of the holes, $\gamma v = p/m_H$, maximizing energy and final black hole spin for values about the critical initial linear momentum separating the direct merger from scattering of the holes.

Typically, for our simulations, we use a grid with global resolution n100 and with 10 levels of refinement, the coarsest of which has resolution of $4M$ and outer boundary of $r = 400M$, with each successive grid with twice the resolution. If we label the coarsest grid $n = 0$, and the finest grid $n = 9$, the resolution on a given level is $M/2^{(n-1)}$. The wavezone is $n = 2$ with a resolution of $M/1$ and boundary out to $r = 125M$. The finest grid has a resolution of $M/256$ with a cube of sides of 1.0 centered around each black hole. For higher initial γv , an additional refinement level is added due to the decreasing black hole radius, with a resolution of $M/512$. In [20] we reported several convergence studies of these kind of simulations confirming the accuracy of our base grid and resolutions.

Fig. 2 displays the maximum radiated energy versus the initial γv of the simulations and the impact parameters b as curve levels for $s = -0.8, 0.0, +0.8$. We have performed this search using 294, 253 and 222 simulations for spins $s = -0.8, 0.0, +0.8$ respectively. We observe a relatively weak dependence on the values of the spins, particularly for the counteraligned and zero spins while a lower maximum is found for the aligned spins with respect to the orbital angular momentum.

In order to consider the effects of the initial data radiation content in Fig. 3 we display the effects of the removal of the initial burst of spurious radiation on the evaluation of the maximum radiated energy.

Table I provides some numerical detail of the subtraction of the spurious radiation from the initial data to extract the more physical gravitational radiation from the high energy collision of the two black holes.

We observe that while the initial burst of radiation is significant, due to both, the presence of spin and rela-

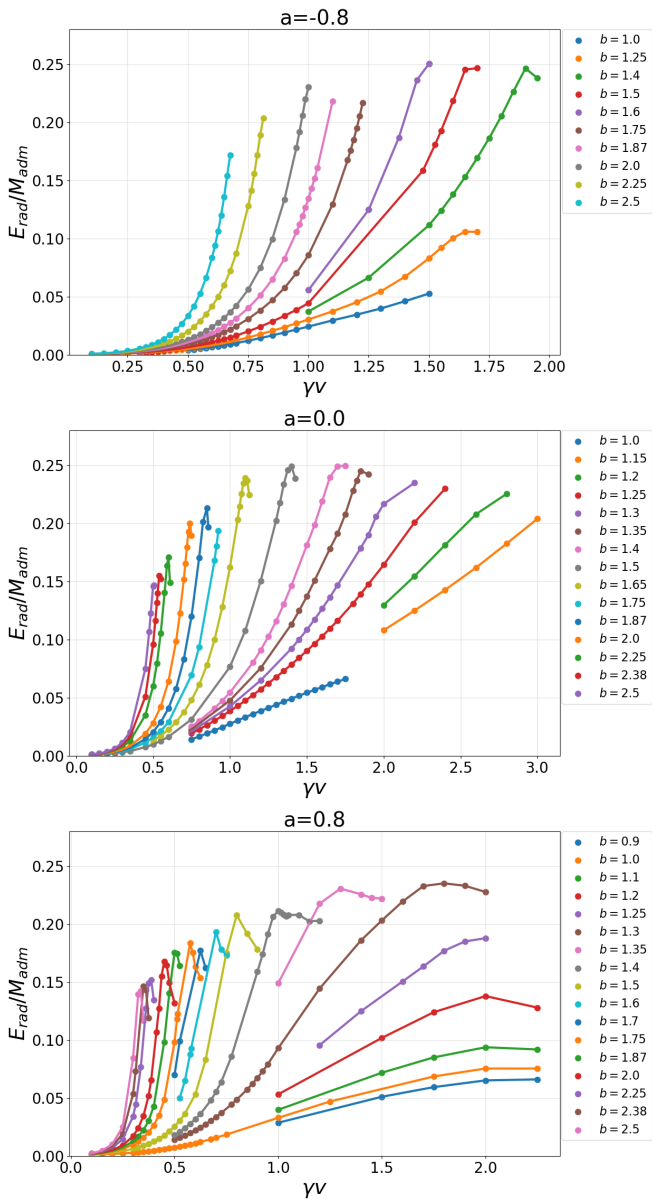


FIG. 2. Maximum E_{rad}/M_{ADM} for different initial momenta parameters γv and impact parameters b for $s = -0.8, 0.0, +0.8$.

tivistic velocities of the holes being simply modeled by the conformally flat Bowen-York ansatz, it is an order of magnitude smaller than the total energy radiated and does not significantly shifts the values of γv and b that lead to its maximum.

A. Numerical convergence targeted studies

Given the large amount of simulations needed to establish the region of parameters that may lead to the largest energy radiated we have assumed a hierarchical approach by first locating the near region of the maximum E_{rad} in

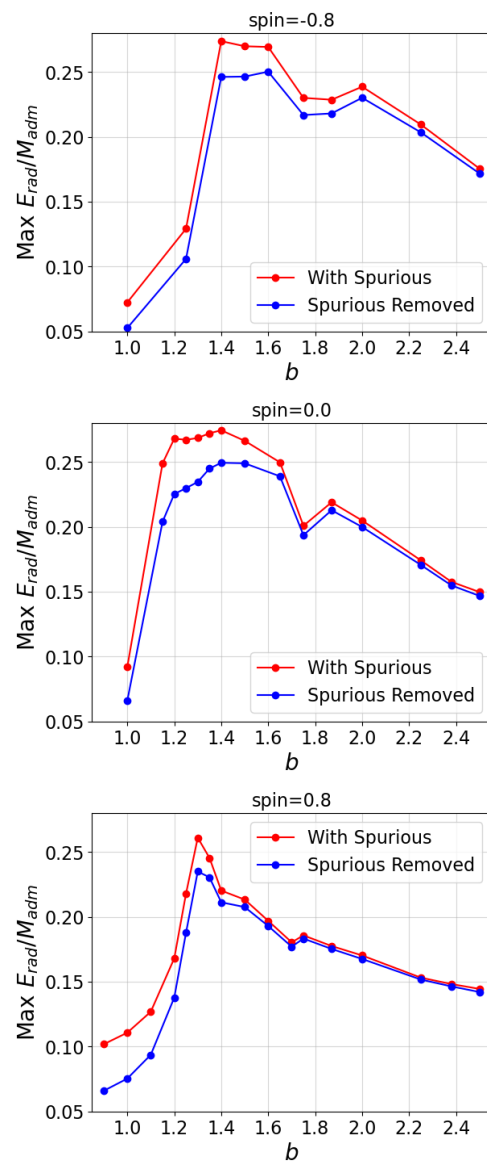


FIG. 3. Maximum E_{rad}/M_{ADM} with removal of the initial burst of radiation for different initial momenta parameters γv and impact parameters b for $s = -0.8, 0.0, +0.8$.

the $(b, \gamma v)$ parameter space with low resolution runs, i.e. n100, and then explore this region with targeted higher resolution simulations that allow us to verify our hierarchical hypothesis as well as providing us with a means to extrapolate in the convergence regime to infinite resolution values.

To explicitly display this procedure we consider the $s = 0$ case by supplementing the n100 simulations with n120 and n144 on by successively increasing the global finite differences resolutions by factors of 1.2. We have adopted here an improved grid with one additional refinement level, i.e. eleven, and changed the shift parameter η from 2 to 1, hence we rerun the n100 simulations together with the n120 and n144 to obtain the convergence rates

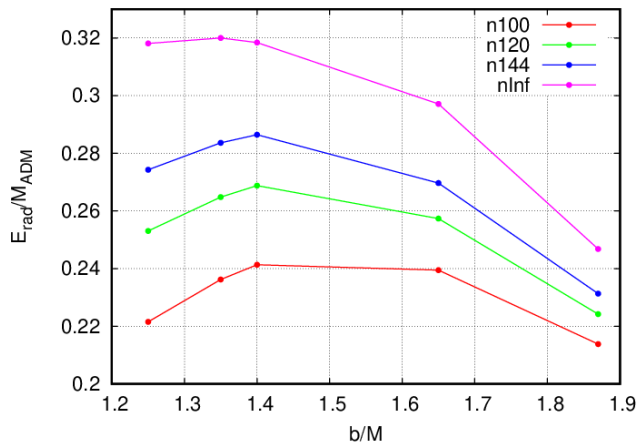


FIG. 4. Maximum E_{rad}/M_{ADM} vs. impact parameter b/M for different numerical resolutions and its extrapolation to infinite resolution ($n_{inf}=n_{\infty}$) for the case $s = 0$.

TABLE II. Dependence of the maximum radiated energy on the parameter (γv) around $s = 0$ maximum for different numerical resolutions (n100,n120,n144) and its extrapolation to infinite resolution n_{∞} with a found convergence order.

b/M	(γv)	n100	n120	n144	n_{∞}	order
1.35	1.850	0.23254	0.26351	0.28297	0.3159	2.54
1.35	1.900	0.23620	0.26479	0.28363	0.3200	2.28
1.35	1.925	0.23635	0.26417	0.28272	0.3198	2.22
1.35	1.950	0.23206	0.25984	0.27851	0.3168	2.17

using formulas (5) in [31]. This sequence is repeated for different values of the impact parameter b/M as displayed in Fig. 4.

Once established the value of $b/M = 1.35$ the analysis is followed up by a verification of the γv dependence around the E_{rad} peak with results as displayed in table II.

A similar process described here for the $s = 0.0$ case is also performed for the $s = \pm 0.8$ cases and the final results are summarized in table III. Thus totaling 30 additional runs in this targeted study in addition to the original 739 of the upper hierarchical search.

While our 769 simulations have been specifically targeted to find the maximum radiated energy covering a large range of black hole spin values, we can also use this set to find out each remnant black hole spin for those cases. In Fig. 5 we show in a histogram form the final

TABLE III. The maximum energy radiated E_{rad}^{max} for spins $0.0, \pm 0.8$. All simulations have equal mass $q = m_1/m_2 = 1$, and were initially placed at $x_{1,2}/M = \pm 25$.

spin	b/M	(γv)	n100	n120	n144	n_{∞}	d
-0.8	1.40	1.900	0.24000	0.26712	0.28587	0.3279	2.02
0.0	1.35	1.900	0.23620	0.26479	0.28363	0.3200	2.29
0.8	1.30	1.800	0.23502	0.26633	0.28416	0.3077	3.09

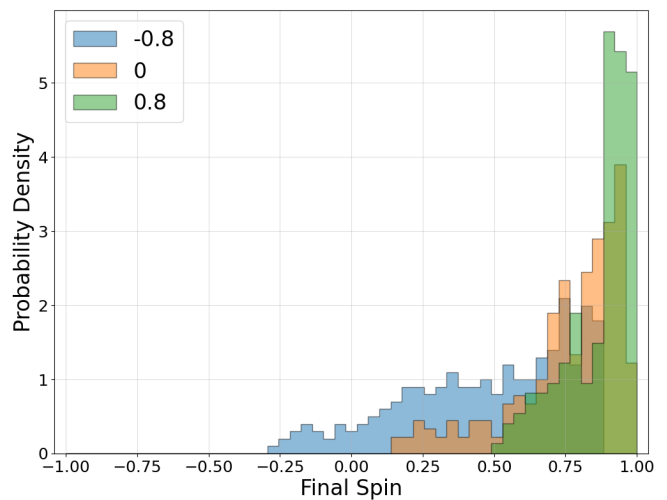


FIG. 5. Normalized histograms for the distributions of final spin calculated from the radiated quantities for the three spin families, $s = -0.8, 0.0, +0.8$ using a number of 294, 253, and 222 simulations respectively.

TABLE IV. Final remnant black hole horizon mass m_f^H and spin α_f^H of the collision case $s = +0.80$, $b = 1.60$, and $\gamma v = 1.15$. For consistent with the radiative quantities also given $M_{ADM} - E_{rad}$ and $J_{ADM} - J_{rad}$, and convergence order.

Resolution	m_f^H	α_f^H	$\frac{(M_{ADM} - E_{rad})}{m_f^H}$	$\frac{(J_{ADM} - J_{rad})}{(m_f^H)^2}$
n144	0.8825	0.98599	0.8899	0.99247
n172	0.8823	0.98636	0.8880	0.99044
n208	0.8822	0.98650	0.8866	0.98720
n_{∞}	0.8821	0.98657	0.8836	-
order	4.2	5.7	2.0	-

merged black hole spin α_f as measured from the radiated quantities for the spin families studied here. By evaluation of the radiated angular momentum and subtracting from the initial ADM angular momentum, we can estimate the spin of the remnant black hole. We clearly see that those binaries with spins aligned with the orbital angular momentum lead to the larger remnant spins, as expected.

From the full pull of simulations we extract the one with the largest remnant spin $\alpha_f = 0.9865$ for case $s = +0.80$, $b = 1.60$, and $\gamma v = 1.15$. In order to verify this near extremely spinning remnant case we perform three additional simulations with increasing resolution as displayed in Table IV showing excellent convergence behavior and where n_{∞} is obtained through extrapolation of the n144, n172, n208 resolutions.

It is worth noting here that unlike the maximum gravitational energy radiated we search for in this paper, the value of the remnant spin $\alpha_f = 0.98657$ only represents a lower bound to the maximum spin achievable by these high energy collisions since we have not seek to fully optimize the parameters to estimate its maximum. It

would be interesting to perform further studies that include near maximal individual spin holes in the direction of the orbital angular momentum to challenge the cosmic censorship hypothesis.

We have also look at the maximum final merger black hole spin when we collide nonspinning holes and have found among our simulations $\alpha_f^{max}(s=0) \approx 0.90$ for $b/M = 1.65$ and $\gamma v = 1.025$.

IV. INITIAL SCATTERING AND SUBSEQUENT CAPTURE AND MERGER

In addition to the direct merging cases we have just discussed, in order to bracket those critical merger impact parameters we performed several simulations showing an initial scattering into elliptic orbits (if the overshooting was too large they would continue in hyperbolic orbits). While in most of our simulations the scattering cases would bounce back from distances at or below $\sim 10M$, it is of interest to discuss in more detail here a couple of cases bouncing at larger separations before merging to illustrate how these can provide additional gravitational radiation besides that produced at the initial close approach passage.

In Fig. 6 we display the scattering case with initial momenta parameters $\gamma v = 1.45$ and impact parameters $b = 1.5$. This configuration approaches until a radius of approximately $0.8M$ before zooming out to about $29M$ and then ultimately merging. This case has unnormalized $M_{ADM} = 1.008$ and individual masses of 0.285 , so around 43% binding energy. It radiates about 21.6% in the first pass and 1.5% afterwards, totaling 23.1%.

In Fig. 7 we display a second scattering case with initial momenta parameters $\gamma v = 1.76$, impact parameters $b = 1.4$, and $M_{ADM} = 1.018$. Individual black hole masses are $0.248M$ each, with the remaining 51% as binding energy. In this case, the black holes reach a separation of $0.7M$, scatter to $41M$, then plunge to merger. This case radiates a total of 23.9%: 22.5% in the first approach and 1.4% in the subsequent merger.

We thus observe that the subsequent radiation by the large eccentricity binary generated by the first encounter while significant, does not compensate enough to overshoot the values of the optimal direct merger cases. This might be due to the less efficient radiation compared to the quasicircular orbits at the same binding energy [32].

V. ZERO FREQUENCY LIMIT EXPANSIONS

The zero frequency limit (ZFL) approximation was introduced by Smarr [21] for the gravitational radiation emitted during the high-energy scattering or collision of two black holes. It was then found that the ZFL not only gives the exact low-frequency results, but that it provides an estimate of the total energy radiated, its spectrum, and its angular distribution when applied to the

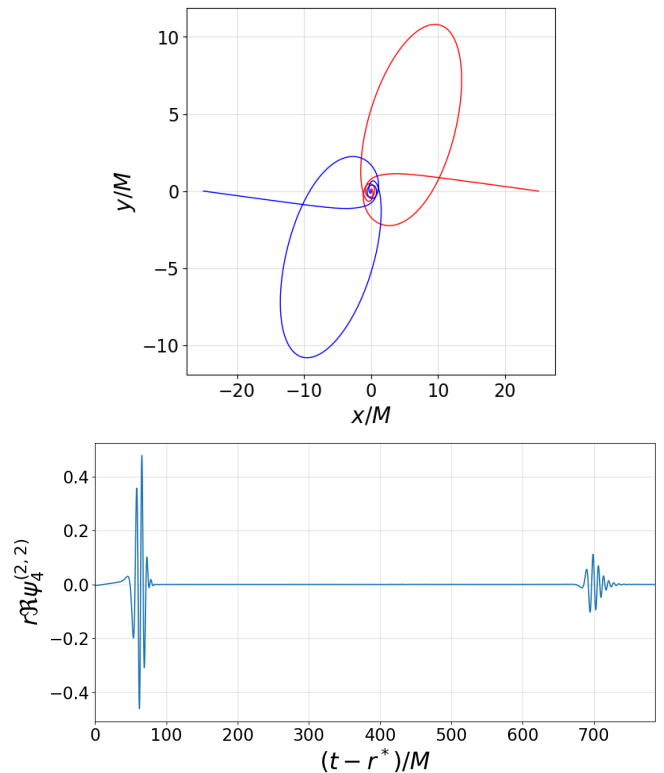


FIG. 6. Trajectories in the orbital plane and $\Re\psi_4^{(2,2)}$ (at $R_{obs} = 75M$) for nonspinning binaries with initial momenta parameters $\gamma v = 1.45$ and impact parameters $b = 1.5$.

high-velocity collision of two particles in a linearized approximation [33].

In this section we expand the computation performed in Ref. [15] to higher orders in the impact parameter b . In our model the two black holes will be treated as point particles initially moving towards each other from the x -axes with impact parameter b . In the center of momentum frame we can write the coordinates explicitly as

$$\begin{aligned} x_k &= (t, vt\lambda_k, \lambda_k\xi_k, 0), \\ p_k &= \gamma_k M_k (1, v\lambda_k, 0, 0), \\ k &= 1, 2 \quad \lambda_1 = 1 \quad \lambda_2 = -1. \end{aligned} \quad (1)$$

with

$$\begin{aligned} \xi_1 + \xi_2 &= b \\ M_1 v_1 \gamma_1 &= M_2 v_2 \gamma_2 \end{aligned} \quad (2)$$

At the closest approach of the holes we set time $t = 0$ and the two particles start orbiting around each other in a circular orbit so that the position and momentum of the particles are written as

$$\begin{aligned} x'_k &= (t, \lambda_k \xi_k \sin \Omega t, \lambda_k \xi_k \cos \Omega t, 0), \\ p'_k &= (t, \lambda_k v_k \cos \Omega t, -\lambda_k v_k \sin \Omega t, 0), \\ k &= 1, 2 \quad \lambda_1 = 1 \quad \lambda_2 = -1. \end{aligned} \quad (3)$$

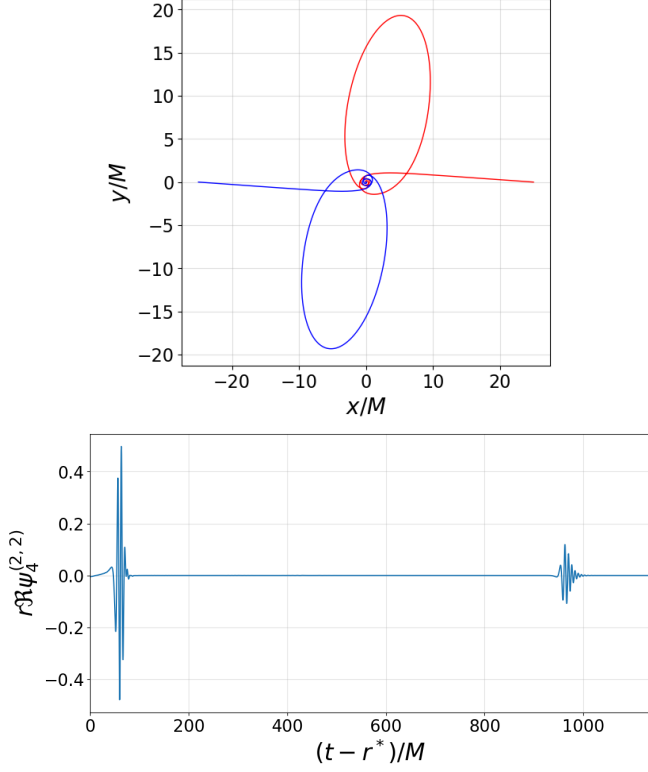


FIG. 7. Trajectories in the orbital plane and $\Re\psi_4^{(2,2)}$ (at $R_{obs} = 75M$) for nonspinning binaries with initial momenta parameters $\gamma v = 1.76$ and impact parameters $b = 1.4$.

with

$$\Omega = \frac{\gamma_1 M_1 v_1 \xi_1 + \gamma_2 M_2 v_2 \xi_2}{\gamma_1 M_1 \xi_1^2 + \gamma_2 M_2 \xi_2^2}. \quad (4)$$

The Fourier transform of the energy-momentum tensor $T^{\mu\nu}(\mathbf{k}, \omega)$ is written as

$$T^{\mu\nu}(\mathbf{k}, \omega) = \frac{1}{2\pi} \int d^4x T^{\mu\nu}(\mathbf{x}, t) e^{i(\omega t - \mathbf{k} \cdot \mathbf{x})}, \quad (5)$$

with $T^{\mu\nu}(\mathbf{x}, t)$ for a point particle given by

$$T^{\mu\nu}(\mathbf{x}, t) = \frac{p_k^\mu p_k^\nu}{\gamma_k M_k} \delta(\mathbf{x} - \mathbf{x}_k(t)). \quad (6)$$

Thus we have

$$\begin{aligned} T^{\mu\nu}(\mathbf{k}, \omega) &= \int d^4x \frac{p_k^\mu p_k^\nu}{\gamma_k M_k} e^{i(\omega t - \mathbf{k} \cdot \mathbf{x})} \delta(\mathbf{x} - \mathbf{x}_k(t)) \Theta(-t) \\ &+ \int d^4x \frac{p_k^\mu p_k^\nu(t)}{\gamma_k M_k} e^{i(\omega t - \mathbf{k} \cdot \mathbf{x})} \delta(\mathbf{x} - \mathbf{x}'_k(t)) \Theta(t) \\ &= \int_{-\infty}^0 dt \frac{p_k^\mu p_k^\nu}{\gamma_k M_k} e^{i(\omega t - \mathbf{k} \cdot \mathbf{x}_k(t))} \\ &+ \int_0^{\infty} dt \frac{p_k^\mu p_k^\nu(t)}{\gamma_k M_k} e^{i(\omega t - \mathbf{k} \cdot \mathbf{x}'_k(t))}. \end{aligned} \quad (7)$$

As we have seen from the full numerical simulations, the effect of the spins of the holes in determining the maximum radiated energy is weak, so for the sake of the simplicity we will focus here in the nonspinning case.

In this case we have

$$\frac{dE_{rad}}{d\omega d\Omega} = 2\omega^2 \left(T^{\mu\nu} T_{\mu\nu}^* - \frac{1}{2} T_\lambda^\lambda T_{\lambda}^{\lambda*} \right). \quad (8)$$

While for the linear momentum radiated we have

$$\frac{dP_{rad}^i}{d\omega} = \int d\Omega \frac{d^2 E_{rad}}{d\omega d\Omega} n_i, \quad (9)$$

where n_i is the unit vector pointing in the i direction.

A similar expression to Eq. (8) can be found for the angular momentum which reads

$$\frac{dJ_{rad}}{d\omega d\Omega} = 2i\omega \frac{d}{d\phi} \left(T^{\mu\nu} T_{\mu\nu}^* - \frac{1}{2} T_\lambda^\lambda T_{\lambda}^{\lambda*} \right). \quad (10)$$

We note that it is trivial to show from this expression that the imaginary terms once integrated over the solid angle contribute only as surface terms which are all 0 because the functions involved are periodic on the sphere.

A. Equal masses

From the detailed computations described in appendix A for the equal mass case $M_1 = M_2 = M/(2\gamma)$, $\xi_1 = \xi_2 = b/2$, $v_1 = v_2 = v$, $\gamma_1 = \gamma_2 = \gamma = (1 - v^2)^{-1/2}$, $\Omega = v/\xi$, the final result for the radiated energy after integrating over the solid angle Ω is

$$\begin{aligned}
\frac{dE_{rad}}{d\omega} = & \frac{(b\omega)^6 M^2}{8670412800\pi v^7} \left[-258048v^{11} + 1507556v^9 - 6216210v^7 + 13531595v^5 + 5358500v^3 \right. \\
& \left. - 525(v^2 - 1)^2 (1396v^6 - 3950v^4 + 4245v^2 - 3577) \tanh^{-1}(v) - 1877925v \right] \\
& + \frac{(b\omega)^4 M^2}{2764800\pi v^5} \left[2560v^9 - 10716v^7 + 34185v^5 + 27270v^3 + 45(v^2 - 1)^2 (204v^4 - 281v^2 + 195) \tanh^{-1} v - 8775v \right] \\
& + \frac{(b\omega)^2 M^2 \left[4v^5 + 27v^3 - 3(v^2 - 1)^2 (4v^2 - 3) \tanh^{-1}(v) - 9v \right]}{144\pi v^3} \\
& + \frac{M^2 \left[(v^4 + 2v^2 - 3) \tanh^{-1} v - v(v^2 - 3) \right]}{2\pi v} + \mathcal{O}(b\omega)^7,
\end{aligned} \tag{11}$$

representing an expansion valid for low impact parameter and frequency combination of the form $b\omega$.

Note that the v -dependence can be converted to the γv variable used in the full numerical simulations by the substitution $v = (\gamma v)/\sqrt{1 + (\gamma v)^2}$.

VI. FITTING ZFL TO SIMULATIONS

Here we will try to fit the energy radiated by high energy collisions with the ZFL dependence on the impact parameter b with coefficients depending on the linear momentum per mass γv from Eq. (11), which we can thus represent symbolically as

$$\frac{E_{rad}}{M_{ADM}} = Af_0(\gamma v) + Bb^2 f_2(\gamma v) + Cb^4 f_4(\gamma v) + Db^6 f_6(\gamma v), \tag{12}$$

where the functional form can be read off Eq. (11) with $v = \gamma v/\sqrt{1 + (\gamma v)^2}$, and the fitting constants include an integration over frequencies from $\omega = 0$ to an effective one ω_{cutoff} .

Notably, when we attempted to fit this dependence to the 229 n100 simulations of equal-mass nonspinning high energy collisions, we first observed the fitting curves produced did not reach above 20% of radiated energies, while we have plenty of simulations that reached up to 25%. We then reduced successively the simulations to include up to $E_{rad}/M_{ADM} \leq 17\%$ and then to $E_{rad}/M_{ADM} \leq 10\%$ not finding statistically very satisfactory fittings until we reduced to 55 simulations producing $E_{rad}/M_{ADM} \leq 5\%$. The results of the fit are reported in Table V. These results suggests that the form of the complete formula applies to small impact parameters only, since we Taylor expanded the approximation in this b parameter.

The result of the fitting is also displayed in Fig. 8 where the residuals appear to be within acceptable bounds.

Since we noticed that the fitting value of the A coefficient is very close to the value 0.5 while that of the

TABLE V. Four Parameter fit with $E_{rad}/M_{ADM} < 0.05$. This fit has 51 degrees of freedom, an rms of 0.00196 and an reduced chisquare of $3.83e - 6$.

parameters	fit	Standard	Error
A	0.492287	+/- 0.02177	(4.422%)
B	0.438939	+/- 0.02512	(5.722%)
C	-0.0360698	+/- 0.009223	(25.57%)
D	0.00115327	+/- 0.000455	(39.45%)

TABLE VI. Two Parameter fit with $E_{rad}/M_{ADM} < 0.05$. This fit has 53 degrees of freedom, an rms of 0.00205, and a reduced chisquare of $4.2e - 6$.

parameters	fit	Standard	Error
B	0.417117	+/- 0.01174	(2.814%)
C	-0.0200655	+/- 0.005073	(25.28%)

coefficient D is very close to 0, we have attempted a new fit by fixing those values and the result is reported in Table VI. This approach produces a further improvement for the relative errors of fitting parameters B and C .

A further simplification can be assumed for the final formula by choosing the simple expressions $A = 1/2$, $B = \sqrt{2} - 1$, $C = 0$, and $D = 0$. Thus producing our final formula as,

$$\frac{E_{rad}}{M_{ADM}} = \frac{1}{2} f_0(\gamma v) + (\sqrt{2} - 1) b^2 f_2(\gamma v), \tag{13}$$

where

$$\begin{aligned}
f_0(\gamma v) = & \frac{1}{2\pi} \left[\frac{3 + 2(\gamma v)^2}{1 + (\gamma v)^2} + \right. \\
& \left. - \frac{(3 + 4(\gamma v)^2) \ln(\gamma v + \sqrt{1 + (\gamma v)^2})}{(1 + (\gamma v)^2)^{3/2} \gamma v} \right] \tag{14}
\end{aligned}$$

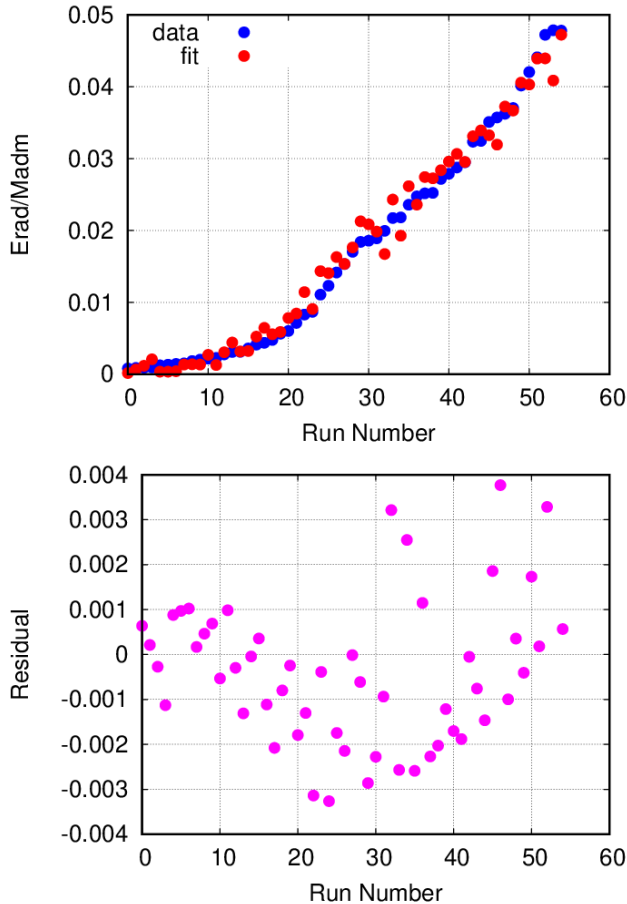


FIG. 8. The 4 parameter fit on the restricted data set ($E_{rad}/M_{ADM} < 0.05$) compared to the actual E_{rad} measured in the 55 simulations for nonspinning high energy collisions and its residuals.

and

$$f_2(\gamma v) = \frac{1}{144\pi(\gamma v)^2} \left[\frac{22(\gamma v)^4 + 9(\gamma v)^2 - 9}{1 + (\gamma v)^2} + \frac{(3(\gamma v)^2 - 9) \ln(\gamma v + \sqrt{1 + (\gamma v)^2})}{\gamma v} \right], \quad (15)$$

to be applied in the small (b/M) regime where the expansion has been fit.

VII. CONCLUSIONS AND DISCUSSION

In this paper we have made a comprehensive search for the maximum gravitational energy of black hole collisions at relativistic speeds finding an estimate of about 1/3 of its total mass. This result is in rough agreement with the previous numerical estimates [34] of around 35%, and we have also confirmed the relatively weak dependence

on the spins of the black holes of the radiated energy, in contrast with the strong spin dependence of the net radiated linear momentum [35], leading to a maximum of $v/c \sim 1/10$ recoil velocities or the maximum spin of the remnant black hole as shown in Fig. 5 for aligned spins merging holes. These results for the maximum possible energy radiated are still below the 45% of using the area bounds [5], final merged black hole horizon mass estimates may be closer to this value and perhaps even further [18, 36] for ultrarelativistic cases.

We have found here that the maximum energy radiated from relativistic speed collisions lead to (at least) one third of its total mass, that is a factor about three larger than the maximum radiated energy from quasicircular orbits [37, 38] for (near) maximally spinning black holes. We also recall here that while the high energy collision of spinning holes lead to a maximum recoil velocity of its merger remnant of about one tenth the speed of light [35], their quasicircular merger is limited by about a sixth of this value [39], i.e. 5000 km/s .

We have been also able to identify in the pool of our initial 739 simulations the one that lead to the highest final remnant spin and produced a further set of higher resolution runs with the same b and γv to extract an accurate horizon measure of $\alpha_f = 0.98657$. As our families of simulations did not necessarily seek for the maximum remnant spin, this represents a lower bound to it. In particular, this simulation selected one with the spins aligned to the orbital angular momentum, but with $s = +0.8$ that is still far from the extreme case $s \rightarrow 1$. This $s \rightarrow 1$ extreme case cannot be explored with Bowen-York-like conformally flat data, that is limited to $v < 0.9c$ [12] and to $s < 0.93$ [40], but needs to be explored with the initial data proposed in [13, 38] that can reach both, black holes with very high spins and very highly relativistic speeds and thus may even explore the cosmic censorship hypothesis. These studies go beyond the scope of the current paper and will be postponed to a new forthcoming research work.

ACKNOWLEDGMENTS

The authors gratefully acknowledge the National Science Foundation (NSF) for financial support from Grant No. PHY-2207920. Computational resources were provided by the Blue Sky, Green Prairies, and White Lagoon clusters at the CCRG-Rochester Institute of Technology, which were supported by NSF grants No. PHY-1229173, No. PHY-1726215, and No. PHY-2018420. This work also used the ACCESS computational resources from the allocation PHY060027, and project PHY20007 in Frontera, an NSF-funded Petascale computing system at the Texas Advanced Computing Center. We thanks Robert Caldwell for pointing out typos en Section V.

- [1] V. Cardoso, L. Gualtieri, C. Herdeiro, U. Sperhak, P. M. Chesler, L. Lehner, S. C. Park, H. S. Reall, C. F. S. (section coordinators), D. Alic, O. J. C. Dias, R. Emparan, V. Ferrari, S. B. Giddings, M. Godazgar, R. Gregory, V. E. Hubeny, A. Ishibashi, G. Landsberg, C. O. Lousto, D. Mateos, V. Moeller, H. Okawa, P. Pani, M. A. Parker, F. Pretorius, M. Shibata, H. Sotani, T. Wiseman, H. Witek, N. Yunes, and M. Zilhão, *Class. Quant. Grav.* **29**, 244001 (2012), arXiv:1201.5118 [hep-th].
- [2] E. Berti, V. Cardoso, L. C. B. Crispino, L. Gualtieri, C. Herdeiro, and U. Sperhake, *Int. J. Mod. Phys. D* **25**, 1641022 (2016), arXiv:1603.06146 [gr-qc].
- [3] V. Cardoso, L. Gualtieri, C. Herdeiro, and U. Sperhake, *Living Rev. Relativity* **18**, 1 (2015), arXiv:1409.0014 [gr-qc].
- [4] S. W. Hawking, *Phys. Rev. Lett.* **26**, 1344 (1971).
- [5] D. M. Eardley and S. B. Giddings, *Phys. Rev.* **D66**, 044011 (2002), arXiv:gr-qc/0201034 [gr-qc].
- [6] M. Siino, *Int. J. Mod. Phys.* **D22**, 1350050 (2013), arXiv:0909.4827 [gr-qc].
- [7] G. Franciolini, A. Maharana, and F. Muia, *Phys. Rev. D* **106**, 103520 (2022), arXiv:2205.02153 [astro-ph.CO].
- [8] Q. Ding, *Phys. Rev. D* **104**, 043527 (2021), arXiv:2011.13643 [astro-ph.CO].
- [9] R.-G. Cai and S.-J. Wang, *Phys. Rev. D* **101**, 043508 (2020), arXiv:1910.07981 [astro-ph.CO].
- [10] U. Sperhake, V. Cardoso, F. Pretorius, E. Berti, and J. A. Gonzalez, *Phys. Rev. Lett.* **101**, 161101 (2008), arXiv:0806.1738 [gr-qc].
- [11] U. Sperhake, E. Berti, V. Cardoso, and F. Pretorius, *Phys. Rev. Lett.* **111**, 041101 (2013), arXiv:1211.6114 [gr-qc].
- [12] J. Healy, I. Ruchlin, C. O. Lousto, and Y. Zlochower, *Phys. Rev.* **D94**, 104020 (2016), arXiv:1506.06153 [gr-qc].
- [13] I. Ruchlin, J. Healy, C. O. Lousto, and Y. Zlochower, *Phys. Rev.* **D95**, 024033 (2017), arXiv:1410.8607 [gr-qc].
- [14] M. Shibata, H. Okawa, and T. Yamamoto, *Phys. Rev.* **D78**, 101501 (2008), arXiv:0810.4735 [gr-qc].
- [15] E. Berti, V. Cardoso, T. Hinderer, M. Lemos, F. Pretorius, *et al.*, *Phys. Rev.* **D81**, 104048 (2010), arXiv:1003.0812 [gr-qc].
- [16] U. Sperhake, W. Cook, and D. Wang, *Phys. Rev. D* **100**, 104046 (2019), arXiv:1909.02997 [gr-qc].
- [17] G. Bozzola, *Phys. Rev. Lett.* **128**, 071101 (2022), arXiv:2202.05310 [gr-qc].
- [18] D. N. Page, *Phys. Rev. D* **107**, 064057 (2023), arXiv:2212.03890 [gr-qc].
- [19] P. E. Nelson, Z. B. Etienne, S. T. McWilliams, and V. Nguyen, *Phys. Rev. D* **100**, 124045 (2019), arXiv:1909.08621 [gr-qc].
- [20] J. Healy and C. O. Lousto, (2022), arXiv:2301.00018 [gr-qc].
- [21] L. Smarr, *Phys. Rev.* **D15**, 2069 (1977).
- [22] Y. Zlochower, J. G. Baker, M. Campanelli, and C. O. Lousto, *Phys. Rev.* **D72**, 024021 (2005), arXiv:gr-qc/0505055.
- [23] C. O. Lousto and Y. Zlochower, *Phys. Rev.* **D77**, 024034 (2008), arXiv:0711.1165 [gr-qc].
- [24] M. Campanelli, C. O. Lousto, P. Marronetti, and Y. Zlochower, *Phys. Rev. Lett.* **96**, 111101 (2006), gr-qc/0511048.
- [25] M. Ansorg, B. Brügmann, and W. Tichy, *Phys. Rev.* **D70**, 064011 (2004), gr-qc/0404056.
- [26] J. Thornburg, *Class. Quant. Grav.* **21**, 743 (2004), gr-qc/0306056.
- [27] M. Campanelli, C. O. Lousto, Y. Zlochower, B. Krishnan, and D. Merritt, *Phys. Rev.* **D75**, 064030 (2007), gr-qc/0612076.
- [28] M. Campanelli and C. O. Lousto, *Phys. Rev.* **D59**, 124022 (1999), arXiv:gr-qc/9811019 [gr-qc].
- [29] H. Nakano, J. Healy, C. O. Lousto, and Y. Zlochower, *Phys. Rev.* **D91**, 104022 (2015), arXiv:1503.00718 [gr-qc].
- [30] R. L. Arnowitt, S. Deser, and C. W. Misner, *Gen. Rel. Grav.* **40**, 1997 (2008), arXiv:gr-qc/0405109 [gr-qc].
- [31] C. O. Lousto and J. Healy, *Phys. Rev.* **D100**, 104039 (2019), arXiv:1908.04382 [gr-qc].
- [32] G. Ficarra and C. O. Lousto, (2024), arXiv:2409.18728 [gr-qc].
- [33] P. N. Payne, *Phys. Rev. D* **28**, 1894 (1983).
- [34] U. Sperhake, V. Cardoso, F. Pretorius, E. Berti, T. Hinderer, and N. Yunes, *Phys. Rev. Lett.* **103**, 131102 (2009), arXiv:0907.1252 [gr-qc].
- [35] J. Healy and C. O. Lousto, *Phys. Rev. Lett.* **131**, 071401 (2023), arXiv:2301.00018 [gr-qc].
- [36] D. N. Page, *Gen. Rel. Grav.* **56**, 104 (2024), arXiv:2209.15014 [gr-qc].
- [37] M. A. Scheel, M. Giesler, D. A. Hemberger, G. Lovelace, K. Kuper, M. Boyle, B. Szilágyi, and L. E. Kidder, *Class. Quant. Grav.* **32**, 105009 (2015), arXiv:1412.1803 [gr-qc].
- [38] Y. Zlochower, J. Healy, C. O. Lousto, and I. Ruchlin, *Phys. Rev.* **D96**, 044002 (2017), arXiv:1706.01980 [gr-qc].
- [39] C. O. Lousto and Y. Zlochower, *Phys. Rev. Lett.* **107**, 231102 (2011), arXiv:1108.2009 [gr-qc].
- [40] S. Dain, C. O. Lousto, and R. Takahashi, *Phys. Rev.* **D65**, 104038 (2002), arXiv:gr-qc/0201062.
- [41] L. Barack and A. Pound, *Rept. Prog. Phys.* **82**, 016904 (2019), arXiv:1805.10385 [gr-qc].
- [42] A. Nagar, J. Healy, C. O. Lousto, S. Bernuzzi, and A. Albertini, *Phys. Rev. D* **105**, 124061 (2022), arXiv:2202.05643 [gr-qc].

Appendix A: Zero Frequency limit expressions

Here we provide explicit expressions for the energy, angular and linear momenta radiated in the ZFL approximation when the two black holes have unequal masses. Potential applications are to model full numerical simulation of comparable masses and also provide the small mass ratio limit explicitly to compare with other approximations like the self-force approach [41] or the EOB studies [42].

1. Tensorial computations for the nonspinning case

In this section we explain in more detail how we evaluated the energy-momentum tensor $T^{\mu\nu}(\mathbf{k}, \omega)$.

We compute separately the two integrals in Eq. (7) as they require different techniques.

Since p_k^μ is independent from t when $t < 0$, the first integral can be computed simply as

$$\begin{aligned} & \int_{-\infty}^0 dt \frac{p_k^\mu p_k^\nu}{\gamma_k M_k} e^{i(\omega t - \mathbf{k} \cdot \mathbf{x}_k(t))} = \\ & = \frac{p_k^\mu p_k^\nu}{\gamma_k M_k i\omega (1 - v_k \lambda_k \sin \theta \cos \phi)} e^{-i\lambda_k \xi_k \omega \sin \theta \sin \phi}. \end{aligned} \quad (\text{A1})$$

For $t > 0$

$$\begin{aligned} & \int d^4x \frac{p_k'^\mu(t) p_k'^\nu(t)}{\gamma_k M_k} e^{i(\omega t - \mathbf{k} \cdot \mathbf{x})} \delta(\mathbf{x} - \mathbf{x}'_k(t)) \Theta(t) = \\ & = \int_0^\infty dt \frac{p_k'^\mu(t) p_k'^\nu(t)}{\gamma_k M_k} e^{i(\omega t - \mathbf{k} \cdot \mathbf{x}'_k(t))}. \end{aligned} \quad (\text{A2})$$

The exponential in Eq. (A2) can be expanded in Bessel functions as

$$\begin{aligned} e^{i\omega t - i\mathbf{k} \cdot \mathbf{x}'_k(t)} & = e^{i\omega t} \exp\{-i\lambda_k \omega \xi_k \sin \theta \sin(\Omega t + \phi)\} = \\ & = e^{i\omega t} \sum_{n=-\infty}^{n=\infty} J_n(-\lambda_k \omega \xi_k \sin \theta) e^{in\Omega t + in\phi}, \end{aligned} \quad (\text{A3})$$

so that Eq. (A2) becomes

$$\begin{aligned} & \int_0^\infty dt \frac{p_k'^\mu(t) p_k'^\nu(t)}{\gamma_k M_k} e^{i(\omega t - \mathbf{k} \cdot \mathbf{x}'_k(t))} = \\ & = \sum_{n=-\infty}^{n=\infty} J_n(-\lambda_k \omega \xi_k \sin \theta) \int_0^\infty dt \frac{p_k'^\mu(t) p_k'^\nu(t)}{\gamma_k M_k} e^{i\omega t} e^{in(\Omega t + \phi)}. \end{aligned} \quad (\text{A4})$$

To work out the contribution given to $T^{\mu\nu}(\mathbf{k}, \omega)$ by $T_{\text{tens}}^{\mu\nu}(\mathbf{x}, t)$ in Eq. (28) of Ref. [15] we use the fact that $T_{\text{tens}}^{\mu\nu}(\mathbf{x}, t)$ can be written as

$$T_{\text{tens}}^{\mu\nu}(\mathbf{x}, t) = \tilde{T}^{\mu\nu}(t) \delta(\cos \theta) \Theta(t) \sum_{k=1}^2 \tau_k(r) \delta(\phi + \Omega t - \phi_k), \quad (\text{A5})$$

where $\tau_k(r)$ is given by Eq. (27) of Ref. [15], $\tilde{T}^{\mu\nu}(t)$ is some tensor depending only on t and $\phi_1 = \frac{\pi}{2}$ and $\phi_2 = \frac{3}{2}\pi$.

Now, using that

$$\begin{aligned} e^{i\omega t - i\mathbf{k} \cdot \mathbf{x}'} & = \\ e^{i\omega t} \exp\{-ir\omega \sin \theta' \sin \theta \cos(\phi - \phi') - ir\omega \cos \theta \cos \theta'\}, \end{aligned} \quad (\text{A6})$$

we find

$$\begin{aligned} & \frac{1}{2\pi} \int d^4x' T_{\text{tens}}^{\mu\nu}(\mathbf{x}, t) e^{i\omega t - i\mathbf{k} \cdot \mathbf{x}} = \\ & = \frac{1}{2\pi} \sum_{k=1}^2 \int_0^\infty dt' \tilde{T}^{\mu\nu}(t) \int_0^\infty dr' r'^2 \tau_k(r') \int_{-1}^1 dx' \delta(x') \\ & \times \int_0^{2\pi} d\phi' \delta(\phi' + \Omega t - \phi_k) e^{i\omega t - i\mathbf{k} \cdot \mathbf{x}'} \\ & = \frac{1}{2\pi} \sum_{k=1}^2 \int_0^\infty dt \tilde{T}^{\mu\nu}(t) e^{i\omega t} \\ & \times \int_0^\infty dr r^2 \tau_k(r) \exp\{-ir\omega \sin \theta \cos((\phi + \Omega t) - \phi_k)\} \\ & = \frac{1}{2\pi} \sum_{k=1}^2 \frac{M_k \xi_k \Omega^2}{\sqrt{1 - (\Omega \xi_k)^2}} \int_0^\infty dt \tilde{T}^{\mu\nu}(t) e^{i\omega t} \\ & \times \int_0^{\xi_k} dr \exp\{-ir\lambda_k \omega \sin \theta \sin(\phi + \Omega t)\}. \end{aligned} \quad (\text{A7})$$

Using again the previous expansion in Bessel functions we find

$$\begin{aligned} & \frac{1}{2\pi} \int d^4x' T_{\text{tens}}^{\mu\nu}(\mathbf{x}, t) e^{i\omega t - i\mathbf{k} \cdot \mathbf{x}} \\ & = \frac{1}{2\pi} \sum_{k=1}^2 \frac{M_k \xi_k \Omega^2}{\sqrt{1 - (\Omega \xi_k)^2}} \sum_{n=-\infty}^{\infty} \left(\int_0^\infty dt \tilde{T}^{\mu\nu}(t) e^{i\omega t + in(\Omega t + \phi)} \right) \\ & \times \int_0^{\xi_k} dr J_n(-r\lambda_k \omega \sin \theta), \end{aligned} \quad (\text{A8})$$

since the components $T^{\mu t}(\mathbf{k}, \omega)$ can be computed from

$$T^{tt}(\mathbf{k}, \omega) = \hat{k}^i \hat{k}^j T_{ij}(\mathbf{k}, \omega), \quad (\text{A9})$$

and

$$T^{ti}(\mathbf{k}, \omega) = \hat{k}^j T_{ij}(\mathbf{k}, \omega). \quad (\text{A10})$$

Thus we can focus on the computation of only the spatial components of the energy-momentum tensor and our final expression reads

$$\begin{aligned} T^{ij}(\mathbf{k}, \omega) & = \\ & \frac{1}{2\pi} \sum_{k=1}^2 \left\{ \frac{p_k^i p_k^j}{\gamma_k M_k i\omega (1 - v_k \lambda_k \sin \theta \cos \phi)} e^{-i\lambda_k \xi_k \omega \sin \theta \sin \phi} \right. \\ & + \sum_{n=-\infty}^{n=\infty} J_n(-\lambda_k \omega \xi_k \sin \theta) \int_0^\infty dt \frac{p_k'^i(t) p_k'^j(t)}{\gamma_k M_k} e^{i\omega t} e^{in(\Omega t + \phi)} \\ & + \frac{M_k \xi_k \Omega^2}{\sqrt{1 - (\Omega \xi_k)^2}} \left(\sum_{n=-\infty}^{\infty} \left(\int_0^\infty dt \tilde{T}^{ij}(t) e^{i\omega t} e^{in(\Omega t + \phi)} \right) \right. \\ & \left. \left. \times \int_0^{\xi_k} dr J_n(-r\lambda_k \omega \sin \theta) \right) \right\}, \end{aligned} \quad (\text{A11})$$

with

$$\begin{aligned}
\tilde{T}^{xx}(t) &= -\sin^2(\Omega t), \\
\tilde{T}^{yy}(t) &= -\cos^2(\Omega t), \\
\tilde{T}^{xy}(t) &= -\sin(\Omega t) \cos(\Omega t).
\end{aligned}
\tag{A12}$$

This can then be used in Eqs. (8)-(10) to compute radiated quantities as follows next.

2. General case

For generic masses and velocities we find once integrating over the solid angle Eqs. (8)-(10)

$$\begin{aligned}
\frac{dE_{rad}}{d\omega} &= \frac{(b\omega)^4(\gamma_1 M_1 v_1)^2}{345600\pi v_1^6 v_2^6 (v_1 + v_2)^3} \left\{ 2v_1 v_2 (v_1 + v_2) \left[2560v_1^9 v_2^5 - 4v_1^8 (1280v_2^6 + 459v_2^4 + 270v_2^2 - 405) \right. \right. \\
&+ 12v_1^7 v_2 (640v_2^6 + 763v_2^4 + 1480v_2^2 - 1320) + v_1^6 (-5120v_2^8 - 25356v_2^6 - 30135v_2^4 + 21510v_2^2 + 2025) \\
&+ v_1^5 v_2 (2560v_2^8 + 9156v_2^6 + 61095v_2^4 + 98620v_2^2 - 19050) - v_1^4 v_2^2 (1836v_2^6 + 30135v_2^4 + 184550v_2^2 - 25275) \\
&+ 5v_1^3 v_2^3 (3552v_2^4 + 19724v_2^2 - 5055) + 15v_1^2 v_2^4 (-72v_2^4 + 1434v_2^2 + 1685) - 30v_1 v_2^5 (528v_2^2 + 635) + 405v_2^6 (4v_2^2 + 5) \left. \right] \\
&- 30v_1^6 (v_2^2 - 1)^2 (108v_1^4 (v_2^2 + 1) - 12v_1^3 v_2 (39v_2^2 + 79) + 9v_1^2 (12v_2^4 + 67v_2^2 + 15) + v_1 v_2 (-1188v_2^4 + 6117v_2^2 - 1135) \\
&+ v_2^2 (828v_2^4 - 5037v_2^2 + 415)) \tanh^{-1} v_2 - 30(v_1^2 - 1)^2 v_2^6 (108(v_1^2 + 1)v_2^4 - 12v_1 (39v_1^2 + 79)v_2^3 \\
&+ 9(12v_1^4 + 67v_1^2 + 15)v_2^2 + v_1 (-1188v_1^4 + 6117v_1^2 - 1135)v_2 + v_1^2 (828v_1^4 - 5037v_1^2 + 415)) \tanh^{-1}(v_1) \left. \right\} \\
&+ \frac{(b\omega)^2(\gamma_1 M_1 v_1)^2}{36\pi v_1^4 v_2^4 (v_1 + v_2)} \left[v_1 v_2 (2v_1^5 (5v_2^2 - 3) - 6v_1^4 v_2 (v_2^2 - 4) + v_1^3 (-6v_2^4 + 9v_2^2 - 9) + v_1^2 v_2^3 (10v_2^2 + 9) + 24v_1 v_2^4 \right. \\
&- 3v_2^3 (2v_2^2 + 3)) + 3(2(v_1^2 - 4v_1 v_2 + v_2^2) + 3)(v_1^4 (v_2^2 - 1)^2 \tanh^{-1} v_2 + (v_1^2 - 1)^2 v_2^4 \tanh^{-1} v_1) \left. \right] \\
&+ \frac{2(\gamma_1 M_1 v_1)^2}{\pi v_1^3 v_2^3 (v_1 + v_2)} \left[-v_1 v_2 (v_1 + v_2) \left((v_1^2 - 1)v_2^2 - v_1^2 - v_1 v_2 \right) + v_1^3 (v_2^2 - 1)(v_1 v_2^2 + v_1 + 2v_2) \tanh^{-1} v_2 \right. \\
&+ (v_1^2 - 1)v_2^3 (v_1 (v_1 v_2 + 2) + v_2) \tanh^{-1} v_1 \left. \right] + \mathcal{O}((b\omega)^5),
\end{aligned}
\tag{A13}$$

$$\begin{aligned}
\frac{dP_{rad}^x}{d\omega} &= \frac{(\gamma_1 M_1 v_1)^2}{\pi v_1^4 v_2^4 (v_1 + v_2)} \left[v_1 v_2 (v_1 - v_2) (v_1 + v_2) (v_1^2 (v_2^2 - 3) - 5v_1 v_2 - 3v_2^2) \right. \\
&\quad + v_1^4 (v_2^2 - 1) (-v_1 (v_2^2 + 3) + v_2^3 - 5v_2) \tanh^{-1} v_2 + (v_1 - 1) (v_1 + 1) v_2^4 (v_1 (v_1 (v_2 - v_1) + 5) + 3v_2) \tanh^{-1} v_1 \left. \right] \\
&\quad - \frac{(b\omega)^2 (\gamma_1 M_1 v_1)^2}{36 (\pi v_1^5 v_2^5 (v_1 + v_2))} \left[(2(v_1^2 - 4v_1 v_2 + v_2^2) + 3) \right. \\
&\quad (v_1^5 v_2 (5v_2^2 - 3) - 5v_1^3 v_2^5 + 3v_1^5 (v_2^2 - 1)^2 \tanh^{-1} (v_2) - 3(v_1^2 - 1)^2 v_2^5 \tanh^{-1} v_1 + 3v_1 v_2^5) \left. \right] \\
&\quad + \frac{(b\omega)^4 (\gamma_1 M_1 v_1)^2}{345600 \pi v_1^7 v_2^7 (v_1 + v_2)^3} \left\{ 2v_1 v_2 (v_1 - v_2) (v_1 + v_2) \left[12v_1^8 (1280v_2^6 + 153v_2^4 + 90v_2^2 - 135) \right. \right. \\
&\quad - 12v_1^7 v_2 (1280v_2^6 + 343v_2^4 + 1390v_2^2 - 1185) + 3v_1^6 (5120v_2^8 - 34188v_2^6 + 4485v_2^4 - 2430v_2^2 - 675) \\
&\quad + v_1^5 v_2 (-4116v_2^6 + 163145v_2^4 - 105910v_2^2 + 17025) + v_1^4 v_2^2 (1836v_2^6 + 13455v_2^4 + 78640v_2^2 - 8250) \\
&\quad - 5v_1^3 v_2^3 (3336v_2^4 + 21182v_2^2 - 3405) \\
&\quad + 30v_1^2 v_2^4 (36v_2^4 - 243v_2^2 - 275) + 15v_1 v_2^5 (948v_2^2 + 1135) - 405v_2^6 (4v_2^2 + 5) \left. \right] \\
&\quad + 30v_1^7 (v_2^2 - 1)^2 (108v_1^4 (v_2^2 + 1) - 12v_1^3 v_2 (39v_2^2 + 79) + 9v_1^2 (12v_2^4 + 67v_2^2 + 15) \\
&\quad + v_1 v_2 (-1188v_2^4 + 6117v_2^2 - 1135) + v_2^2 (828v_2^4 - 5037v_2^2 + 415)) \tanh^{-1} v_2 \\
&\quad - 30(v_1^2 - 1)^2 v_2^7 (108(v_1^2 + 1)v_2^4 - 12v_1 (39v_1^2 + 79)v_2^3 + 9(12v_1^4 + 67v_1^2 + 15)v_2^2 \\
&\quad + v_1 (-1188v_1^4 + 6117v_1^2 - 1135)v_2 + v_1^2 (828v_1^4 - 5037v_1^2 + 415)) \tanh^{-1} v_1 \left. \right\} + \mathcal{O}((b\omega)^5),
\end{aligned} \tag{A14}$$

$$\begin{aligned}
\frac{dJ_{rad}^z}{d\omega} &= \frac{b(\gamma_1 M_1 v_1)^2}{\pi v_1^3 v_2^3 (v_1 + v_2)^2} \left[-v_1 v_2 (v_1 + v_2) (v_1^3 v_2 (v_2^2 - 3) + v_1^2 (1 - 6v_2^2) + v_1 (v_2 - 3v_2^3) + v_2^2) \right. \\
&\quad + v_1^3 (v_2^2 - 1) (v_1^2 v_2 (v_2^2 + 3) + v_1 (5v_2^2 - 1) + 2v_2 (v_2^2 - 1)) \tanh^{-1} v_2 \\
&\quad + (v_1^2 - 1) v_2^3 (v_1 (v_1^2 (v_2^2 + 2) + 5v_1 v_2 + 3v_2^2 - 2) - v_2) \tanh^{-1} v_1 \left. \right] \\
&\quad - \frac{(b\omega)^2 b(\gamma_1 M_1 v_1)^2}{72 \pi v_1^4 v_2^4 (v_1 + v_2)^2} \left[v_1 v_2 (v_1 + v_2) (32v_1^5 v_2^3 + v_1^4 (-41v_2^4 - 24v_2^2 + 9) + v_1^3 v_2 (32v_2^4 + 27v_2^2 - 135) \right. \\
&\quad - 3v_1^2 (8v_2^4 - 87v_2^2 + 9) + 27v_1 v_2 (1 - 5v_2^2) + 9v_2^2 (v_2^2 - 3)) + 9v_1^4 (v_2^2 - 1)^2 (v_1^2 (v_2^2 - 1) + 14v_1 v_2 - 9v_2^2 + 3) \tanh^{-1} v_2 \\
&\quad + 9(v_1^2 - 1)^2 v_2^4 (v_1^2 (v_2^2 - 9) + 14v_1 v_2 - v_2^2 + 3) \tanh^{-1} v_1 \left. \right] + \mathcal{O}((b\omega)^5).
\end{aligned} \tag{A15}$$

Note that these formulas have been found in the initial center of momentum frame as given in Eq. (1), and there

verify the exchange of the black hole labeling 1 and 2 symmetry.